

Article

Different Types of Continuous Track Irregularities as Sources of Train-Induced Ground Vibration and the Importance of the Random Variation of the Track Support

Lutz Auersch

Department 7 Safety of Structures, Federal Institute of Material Research and Testing, 12200 Berlin, Germany; lutz.auersch-saworski@bam.de

Abstract: Irregularities of the track are a main cause of train-induced ground vibration, and track maintenance is of great importance. Although geometric irregularities at the wheel-rail contact are widely used, other types of irregularities, such as stiffness irregularities, irregularities from different track positions and irregularities in the wave propagation, were analysed in the present study. The track behaviour was investigated by a multi-beam-on-soil model. This track model is coupled with a vehicle model to calculate the vehicle-track interaction. The track model was also used for the track filtering, which transfers a track support error to the equivalent rail irregularity or, conversely, the sharp axle pulse on the rail to a smoother pulse on the soil. In the case in which this filtering varies randomly along the track, the pulses of the moving static load induce a certain ground vibration component (“the scatter of axle pulses”). This effect was calculated by the superposition of axle pulses in the frequency domain and by a stochastic simulation. Simultaneous vehicle, track and soil measurements at a certain site were used to evaluate the different excitation and ground vibration components. The agreement between calculations and axle-box and soil measurements is good. The ground vibrations calculated from rail irregularities and corresponding dynamic loads, however, clearly underestimate the measured ground vibration amplitudes. Only the static load that is moving over a varying track support stiffness can produce the important mid-frequency ground vibration component by the scatter of axle pulses.

Keywords: train-induced ground vibration; geometric vehicle and track irregularities; stiffness variation; multi-beam track model; track filtering; dynamic axle loads; static axle loads; layered soil



Citation: Auersch, L. Different Types of Continuous Track Irregularities as Sources of Train-Induced Ground Vibration and the Importance of the Random Variation of the Track Support. *Appl. Sci.* **2022**, *12*, 1463. <https://doi.org/10.3390/app12031463>

Academic Editors: Araliya Mosleh, José A.F.O. Correia, Diogo Ribeiro and Anna M. Rakoczy

Received: 15 December 2021

Accepted: 25 January 2022

Published: 29 January 2022

Publisher's Note: MDPI stays neutral with regard to jurisdictional claims in published maps and institutional affiliations.



Copyright: © 2022 by the author. Licensee MDPI, Basel, Switzerland. This article is an open access article distributed under the terms and conditions of the Creative Commons Attribution (CC BY) license (<https://creativecommons.org/licenses/by/4.0/>).

1. Introduction

Irregularities are the main source of excitation of train-induced ground vibrations, which are in the frequency range of 4 to 100 Hz (maximal 250 Hz). Irregularities can be divided into vertical, horizontal, rotational and gauge errors; vehicle and track irregularities; and low-frequency alignment errors and high-frequency roughness errors, where the areas of interest of the present article are underlined. The irregularities are presented as wavelength or wavenumber spectra. Some normative alignment spectra from US, China, France, and Germany are presented and compared in [1]. Measurement examples of track errors are given, for example, in [2,3]. The track errors in the present article are based on own axle-box measurements at a ground vibration measurement site [4]. The article is focused on the mid-frequency range of 8 to 30 Hz, which is usually the dominant ground vibration in the mid and far field.

In ground vibration analysis, different numerical models of the railway track and the soil have been established: the wavenumber-domain models [5–8], finite/infinite-element models [9–12] (SBFEM), boundary-element models [13,14], and 2.5D coupled wavenumber-domain (finite or boundary-element) models [5,15–17]. The present contribution is based on frequency-wavenumber methods and their approximations; see Appendix A. The additional method of superposition of axle pulses was also used in [18] for trans-Rayleigh

trains that are moving faster than the waves in the soil; however, these are not included in the present contribution.

When the theoretical models are compared with measurements, the geometric irregularities at the wheel–rail contact are used as the excitation in most cases. Moreover, the irregularities from the US standard [2], which are quite high, are often used. For some model verifications, the irregularities are measured [5,8,17,19] mainly by hand-driven trolleys, which are suitable for roughness and for which the results must be extrapolated to low frequencies. In [19], a low-frequency method was used in addition to the high-frequency roughness measurement and the combined results showed an almost unique curve. Axle-box measurements [4,5] provide results for a wide frequency range and include track and vehicle irregularities that can be distinguished by their different frequency characteristics [20]. In all these cases, the inertial forces of the wheelset running over the irregularities are understood as the excitation of the ground vibration.

In addition to track and vehicle irregularities, the following irregularities can be distinguished: rail unevenness or roughness [21] and wheel unevenness or roughness, which are both at high frequencies above 50 Hz and are not covered in this article; low order wheel out-of-roundness between 10 and 50 Hz [22]; geometric track alignment or level errors, geometric track support errors and track support stiffness variations usually below 30 Hz [23–25]; and deterministic track stiffness variation with sleeper-distance frequency above 50 Hz [26]. All these irregularities generate dynamic axle loads when an axle (the unsprung mass) passes over these irregularities [27]. An additional effect follows from the passage of a static load over a track with an irregular track support (irregular ballast, irregular soil, irregular sleeper contact). The randomly varying track support stiffness was analysed experimentally in [28–30], and it is known that the track support can strongly vary up to hanging sleepers. In the case of varying track stiffness, the ground vibration is generated in a different way by the irregular transfer of the static load to the ground.

The structure of this article is as follows. First (Section 2), the importance of the mid-frequency ground vibration component is illustrated by measurements at two sites. In Section 3, all theoretical methods are described, namely, the track analysis by a multi-beam-on-soil model, the vehicle–track interaction for the force transfer functions, the track filtering for geometric track support errors, a two-step linear perturbation analysis for the support stiffness variation, and the regular and irregular superposition of the axle pulses on all sleepers by a stochastic simulation. In Section 4, the calculated force transfers and ground vibrations for all excitations are presented. Finally, the detailed results (acceleration, irregularity, and force spectra, and ground vibration amplitudes and spectra) of a measurement site are compared with the calculations in Section 5.

2. Experimental Motivation by the Dominant Frequency Range of Railway-Induced Ground Vibration

This article was motivated by experimental observations of railway-induced ground vibration. The ground vibration was measured by geophones (velocity transducers), filtered and amplified, digitised with a frequency of 2 kHz in a 72-channel measurement system. An instrumented impact hammer was used for artificial excitation and yields the force signal to evaluate transfer functions (Section 5.2).

Two examples are shown in Figure 1—the passage of standard passenger trains at site N with soft clayey soil (shear wave velocity $v_S = 150$ m/s), train speed $v_T \approx 100$ km/h, and at site H with sandy, medium stiff soil ($v_S = 225$ m/s) and a train speed of $v_T \approx 160$ km/h. A third site W is analysed in Section 5.3, where a special passenger train was run with specific train speeds between 63 and 160 km/h, at least three times for each speed. The standard trains were measured 10 to 15 times with slightly varying speed.

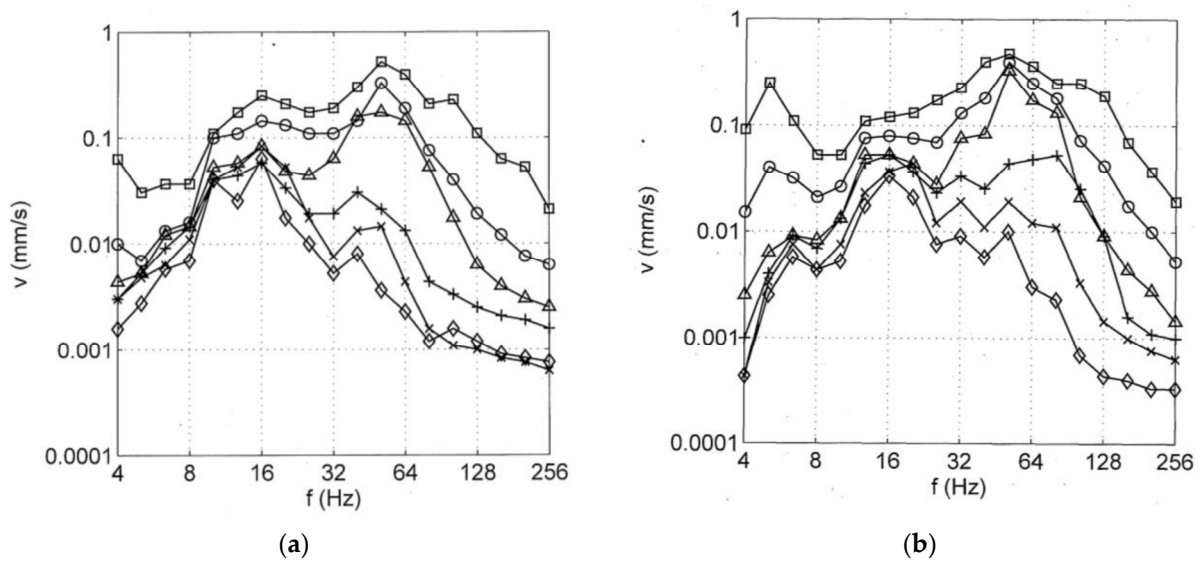


Figure 1. Train induced ground vibration, (a) at site N, (b) at site H, at distances $x = \square 3, \circ 5, \Delta 10, + 20, \times 30,$ and $\diamond 50$ m [20].

The train induced ground vibrations of site N and site H are shown in Figure 1 for the distances between 3 and 50 m as one-third octave band spectra of the whole frequency range from 4 to 256 Hz. The response can be roughly divided into three frequency ranges. The low frequencies have only small amplitudes (except sometimes the first measurement point). The high frequencies have a strong attenuation with distance so that the further distances have small amplitudes. The mid-frequency range from 8 to 30 Hz has a weak attenuation and has therefore the greatest amplitudes in some distance. Therefore, the mid frequencies are the most important frequency range in most situations, and the analysis of the present contribution is focused on this important mid-frequency range.

3. Frequency Domain Methods of Calculation

3.1. Simple Vehicle and Multi-Beam-on-Soil Track

The dynamic stiffness K_V of the vehicle can be approximated by the mass m_W of the wheelset and the circular frequency ω as:

$$K_V(\omega) = -m_W\omega^2 \tag{1}$$

The minor effects of more detailed vehicle models have been discussed in [31].

Many track systems have been calculated by the combined finite-element boundary-element method [32] or by a faster multi-beam-on-soil track model in the frequency-wavenumber domain (Figure 2) as follows. The track model consists of n beams that represent the rails and track slabs, and which are described by the bending stiffnesses EI_j and the masses per length m_j' in the diagonal matrices \mathbf{EI} and \mathbf{M} , and by a stiffness and damping matrix \mathbf{K} and \mathbf{C} representing rail pads, sleepers, the ballast and any isolation element. The multi-beam system fulfils the set of differential equations for the displacements \mathbf{u} and the load (per length) \mathbf{F}'_T :

$$\mathbf{EI} \frac{\partial^4 \mathbf{u}}{\partial y^4} + \mathbf{M} \frac{\partial^2 \mathbf{u}}{\partial t^2} + \mathbf{C} \frac{\partial \mathbf{u}}{\partial t} + \mathbf{K} \mathbf{u} = \mathbf{F}'_T \tag{2}$$

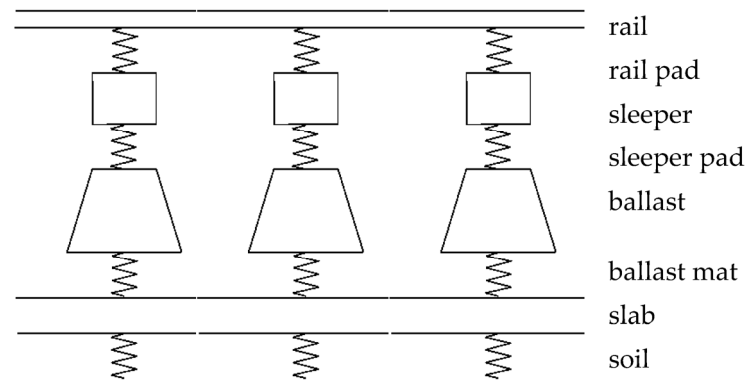


Figure 2. Track model consisting of rail, rail pad, sleeper, sleeper pad, ballast, ballast mat, ballast plate and continuous soil.

This equation is transformed to the frequency-wavenumber domain with wavenumber ζ :

$$(\zeta^4 \mathbf{EI} - \omega^2 \mathbf{M} + i\omega \mathbf{C} + \mathbf{K})\mathbf{u}(\omega, \zeta) = (\zeta^4 \mathbf{EI} + \mathbf{K}_{\text{TS}}(\omega, \zeta))\mathbf{u}(\omega, \zeta) = \mathbf{F}'_{\text{T}}(\omega, \zeta) \quad (3)$$

where $\mathbf{K}_{\text{TS}}(\omega, \zeta) = \mathbf{K}_{\text{T}}(\omega) + \mathbf{K}_{\text{S}}(\omega, \zeta)$ is the dynamic track–soil stiffness matrix. The track stiffness $\mathbf{K}_{\text{T}}(\omega)$ is calculated by transfer matrices for each support element [33], and the soil stiffness $\mathbf{K}_{\text{S}}(\omega, \zeta) = k_{\text{S}}(\omega, \zeta)\mathbf{e}_{\text{n}}^{\text{T}}\mathbf{e}_{\text{n}}$ is added to the last diagonal element. The soil stiffness $k_{\text{S}}(\omega, \zeta)$ is calculated as a wavenumber integral and can be approximated by a Winkler approach $k_{\text{S}}^*(\omega) = k_{\text{W}} + i\omega c_{\text{W}}$ (see Appendix A).

The dynamic track stiffness $K_{\text{T}}(\omega)$ between the axle load F_{T} and the corresponding rail displacement u_{R} can be calculated from the wavenumber integral:

$$\frac{1}{K_{\text{T}}(\omega)} = \frac{u_{\text{R}}}{F_{\text{T}}}(\omega) = \frac{1}{2\pi} \int_{-\infty}^{\infty} \mathbf{e}_1^{\text{T}} (\mathbf{EI}\zeta^4 + \mathbf{K}_{\text{TS}}(\omega, \zeta))^{-1} \mathbf{e}_1 d\zeta \quad (4)$$

The force F_{S} on the soil follows from the displacement u_{S} of the soil and the soil stiffness k_{S} as:

$$F_{\text{S}}(\omega) = k_{\text{S}}u_{\text{S}}(\omega, \zeta = 0) = k_{\text{S}}(\omega, \zeta = 0)\mathbf{e}_{\text{n}}^{\text{T}}\mathbf{K}_{\text{TS}}(\omega, \zeta = 0)^{-1}\mathbf{e}_1 F_{\text{T}} = H_{\text{T}}(\omega)F_{\text{T}}(\omega) \quad (5)$$

The base vector \mathbf{e}_1 stands for the top of the track, the base vector \mathbf{e}_{n} stands for the bottom of the track (the soil).

3.2. The Vehicle-Track Transfer Functions

The dynamic stiffness $K_{\text{T}}(\omega)$ of the track is coupled with the dynamic stiffness $K_{\text{V}}(\omega)$ of the vehicle to analyse the combined vehicle–track system. The force F_{T} that acts on the track is calculated as:

$$F_{\text{T}}(\omega) = -\frac{K_{\text{V}}(\omega)K_{\text{T}}(\omega)}{K_{\text{V}}(\omega) + K_{\text{T}}(\omega)}s(\omega) = H_{\text{V}}(\omega)s(\omega) \quad (6)$$

for the geometric vehicle–track irregularities $s(\omega)$. In the case of a varying track stiffness $K_{\text{T}}(x)$ (see Section 3.4), a similar transfer function $H_{\text{V}}^*(\omega)$ for the effective track irregularities $s^*(\omega)$ yields:

$$F_{\text{T}}(\omega) = -\frac{K_{\text{V}}(\omega)K_{\text{T}0}}{K_{\text{V}}(\omega) + K_{\text{T}}(\omega)}s^*(\omega) = H_{\text{V}}^*(\omega)s^*(\omega) \quad (7)$$

The only difference is that the static track stiffness $K_{\text{T}0}$ is used in the numerator [34]. Equation (7) holds also for the effective irregularity s_{D}^* due to the stiffness variation on and between the sleepers.

In general, the influence of the track mass must be introduced by the force transfer function $H_T(\omega) = F_S/F_T(\omega)$ in Equation (5) from the top to the bottom of the track. Finally, the force F_S on the soil, which excites the ground vibration, can be calculated as:

$$F_S(\omega) = H_T(\omega)F_T(\omega) = H_T(\omega)H_V(\omega)s(\omega). \tag{8}$$

For the standard ballast track and the interesting frequency range (8–30 Hz), the track transfer $H_T(\omega)$ is almost 1, so that the force on the track is nearly the force on the soil $F_T \approx F_S = F$ (the dynamic axle load).

3.3. Irregularities at the Vehicle-Track Interface

The mostly referenced causes of train-induced ground vibrations are geometric irregularities of the vehicle and the track, which are most simply described as geometric irregularities s at the interface between wheel and rail. Irregularities can also come from other positions in the track [23], and, most importantly, from the track support. Moreover, irregularities are not only geometric irregularities, but can also be due to a stiffness variation. All irregularities can be transformed to effective irregularities at rail level s^* , s_R and the dynamic loads follow with the vehicle–track transfer function (6), (7). The effects of the geometric or stiffness variation of the track support are presented in the next section.

3.4. Irregularities of the Track Support and Track Filtering

3.4.1. Geometric Irregularities of the Track Support

At first, the track is excited by a harmonic irregularity of the soil surface:

$$s_S(\xi) = s_S e^{i\xi x} e_n. \tag{9}$$

The response \mathbf{u} to this excitation is also a harmonic function, which can be calculated in wavenumber domain according to [24]:

$$\left(\mathbf{EI}\xi^4 + \mathbf{K}_{T0}(\xi) \right) \mathbf{u} + \mathbf{K}_{S0}(\mathbf{u}(\xi) - s_S(\xi)) = 0 \tag{10}$$

\mathbf{K}_{T0} is the static support stiffness inside the track beams and \mathbf{K}_{S0} is the static support stiffness under the track beams. No external force is present and only the difference $\mathbf{u}-s_S$ yields a force $\mathbf{K}_S(\mathbf{u}-s_S)$ between the track and the soil. The solution is:

$$\begin{aligned} \mathbf{u}(\xi) &= \left(\mathbf{EI}\xi^4 + \mathbf{K}_{T0}(\xi) + \mathbf{K}_{S0}(\xi) \right)^{-1} \mathbf{K}_{S0}(\xi) s_S(\xi) \\ \mathbf{u}(\xi) &= \left(\mathbf{EI}\xi^4 + \mathbf{K}_{TS0}(\xi) \right)^{-1} \mathbf{e}_n k_{S0}(\xi) s_S, \end{aligned} \tag{11}$$

and the effective track irregularity s_R at the rail level is:

$$s_R(\xi) = \mathbf{e}_1^T \left(\mathbf{EI}\xi^4 + \mathbf{K}_{TS0}(\xi) \right)^{-1} \mathbf{e}_n k_{S0}(\xi) s_S = H_{sT}(\omega = \xi v_T) s_S \tag{12}$$

This equation holds in the wavenumber domain and also in the frequency domain if the relation $\omega = \xi v_T$ with train speed v_T is used.

3.4.2. Random Variation of the Track Support Stiffness

Another possible excitation of railway-induced ground vibration is due to the variation of the track support stiffness as:

$$k_S = k_0 + k_1 \exp(i\xi v_T y) \tag{13}$$

with a constant mean stiffness k_0 . The stiffness variation k_1 yields a track response in combination with the static train load F_0 , and:

$$\mathbf{EI} \frac{\partial^4 \mathbf{u}}{\partial y^4} + (\mathbf{K}_0 + \mathbf{K}_1(y)) \mathbf{u} = F_0 \mathbf{e}_1 \delta(y) \tag{14}$$

is the differential equation for the displacements \mathbf{u} along the track. The solution is established by a two-step linear perturbation analysis as $\mathbf{u} = \mathbf{u}_0 + \mathbf{u}_1$ [23,24]. Finally, the effective track irregularity s^* at the rail level is achieved by the transfer function:

$$\frac{s^*}{k_1/k_0}(\omega) = -\frac{F_0 k_0}{2\pi} \int_{-\infty}^{\infty} \mathbf{e}_1^T (\mathbf{EI} \zeta^4 + \mathbf{K}_0)^{-1} \mathbf{e}_n \mathbf{e}_n^T (\mathbf{EI}(\zeta - \zeta_V)^4 + \mathbf{K}_0)^{-1} \mathbf{e}_1 d\zeta = H_{kT}(\omega = \zeta_V v_T) \tag{15}$$

3.5. Superposition of Axle Pulses from Passing Trains

The additional effect of moving static loads is analysed by the pulses on the track. Each wheelset yields a pulse on each sleeper, and all responses of the soil to these pulses are superposed in the frequency domain. First, the general method is described, which can also be applied to a regular track. The case of an irregular track with a varying support stiffness is then solved numerically by a stochastic simulation.

3.5.1. Regular Track Support

The passage of the static train loads is represented by a number of impulses at a line of discrete excitation points y_j . The passage of a train yields impulses $F_0 dt$ on the track due to the static axle load F_0 . The length dt of the impulse follows from the distance dy of the discrete excitation points and the train speed v_T as $dt = dy/v_T$. The impulse on the rail is a Dirac function $\delta(t)$. The bending stiffness of the track filters out the high frequency content of this infinitely sharp impulse. This is expressed by the filter function (Figure 3a):

$$H_F(\omega = \zeta v_T) = \frac{F_S}{F_R} = \mathbf{e}_1^T (\mathbf{EI} \zeta^4 + \mathbf{K}_{TS0})^{-1} \mathbf{e}_n k_s = \frac{s_R}{s_S} = H_{sT}(\omega = \zeta v_T) \tag{16}$$

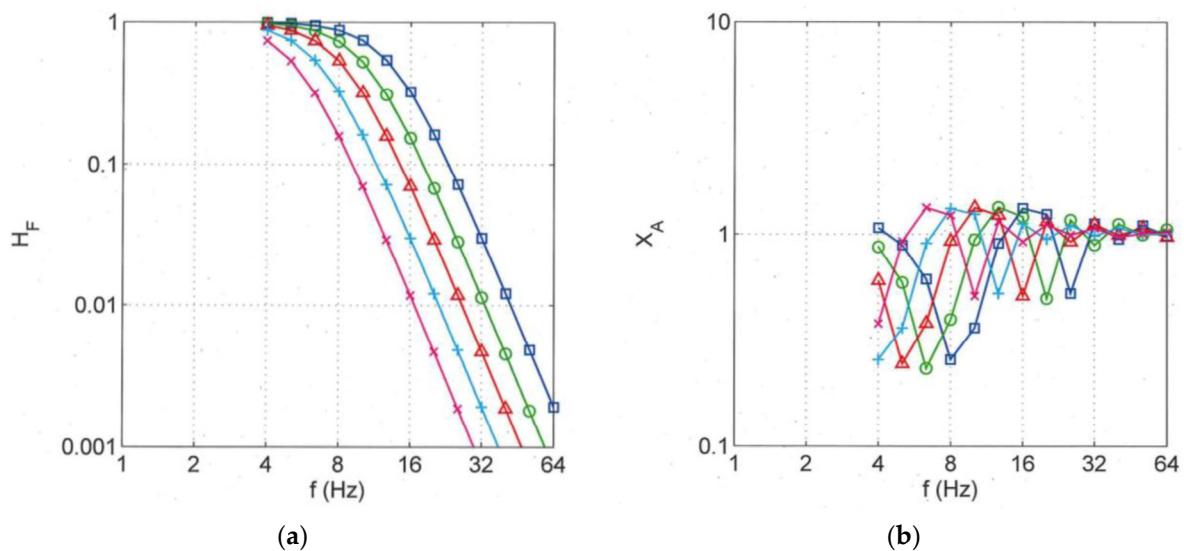


Figure 3. Spectra for the calculation of a standard ballast track with varying track support stiffness, (a) filter function of the track force, (b) axle-sequence spectrum of two axles of a bogie, train speed $\times 63$, $+ 80$, $\Delta 100$, $\circ 125$, and $\square 160$ km/h.

The filter function for the force is the same as the filter function (12) for the geometric track support irregularities due to reciprocity. In the case of a standard ballast track, the filter function is reduced to:

$$H_F(\omega = \zeta v_T) = \frac{k_S}{EI\zeta^4 + k_S} = \frac{1}{1 + (\omega/\omega_0)^4} \tag{17}$$

where the cut-off frequency ω_0 is ruled by the bending stiffness EI of the track, the support stiffness k_S of the ballast and soil, and the train speed v_T according to:

$$\omega_0 \sim \sqrt[4]{\frac{k_S}{EI}} v_T \tag{18}$$

For a ballast track and a train speed of 160 km/h, a frequency of $f_0 = 13$ Hz is used.

The impulses at different places y_j are applied at different times $t_j = y_j/v_T$. The delay time t_j is included in the frequency domain as the factor:

$$\exp(-i\omega t_j) \tag{19}$$

Then the response at a distance x from the track to the sequence of impulses due to a single axle is given as the spectral density:

$$u(x, \omega) = H_F(\omega) F_0 dt \sum_{j=-n/2}^{+n/2} H_S(x, y_j, \omega) \exp(-i\omega t_j) \tag{20}$$

for the displacements and:

$$v(x, \omega) = i\omega u(x, f) \tag{21}$$

for the particle velocities. $H_S(x, y_j, \omega)$ is the transfer function of the soil and is calculated by an infinite integration in the frequency-wavenumber domain (see [35] and Appendix A) and summed for the $n+1$ excitation points y_j . The response of a whole train follows by the multiplication of (21) with the axle-sequence spectrum (Figure 3b):

$$X(f) = \left| \sum_{k=1}^{2n_B} F_k^* \exp(-i\omega T_k) \right| \approx \sqrt{n_B} X_A(f) = \sqrt{n_B} 2 \left| \cos\left(\pi f \frac{2l_B}{v_T}\right) \right| \tag{22}$$

where $n_B (=20)$ is the number of bogies and $2l_B (=2.5 \text{ m})$ is the axle distance in the bogie. The spectrum $X(f)$ of all axles with arrival times T_k and relative static loads $F_k^* (=1)$ can be approximated with the axle-distance spectrum $X_A(f)$ of a single bogie in the frequency range of interest (8–30 Hz). The axle-sequence spectrum $X_A(f)$ has two characteristic minima, which are shifted in frequency with train speed.

The results are presented as one-third of octave band spectra that follow from the spectral densities (20), (21) as:

$$v(x, f_T) = 2 \sqrt{\sum_{l=l_u}^{l_o} \frac{v^2(x, f_l)}{n_T} \sqrt{df df_T}} \tag{23}$$

where f_T is the centre frequency of the one-third of octave band, and f_l are the n_T frequencies of the spectral density within one-third of the octave band ($l_u < l < l_o$). One-third of the octave bands df_T are proportional to the frequency $df_T = 0.23f$ and the linear frequency band $df = 0.5 \text{ Hz}$ is used as the reference.

3.5.2. Randomly Varying Track Support

A soft or stiff track support has an influence on the load distribution of the track. A soft track support yields a wide load distribution, whereas a stiff track support yields a narrow

load distribution. The distribution of the load along the track simultaneously means a distribution of the load in time. The impulses from the static axle loads are sharper for a stiff track support and smoother for a soft track support. The random variation of the track support stiffness is now included in the model in a simplified manner by modifying the width of the impulse. The width of the impulse is expressed in the filter function (17) of the track. A soft track support shifts the filter frequency f_0 to a lower value. The random track support stiffness is realised in the calculation by a random support stiffness and hence a random filter frequency of the track. The stiffness for each excitation point is calculated as:

$$k_S(y_j) = k_0(1 + q \text{rand}(j)) \quad (24)$$

where k_0 is the average value and q is the percentage of the variation, and $\text{rand}(j)$ are equally distributed random numbers between -1 and $+1$. A total of 100 realisations of the stiffness distributions were analysed and the average of the response is presented.

The other calculation parameters are the distance of the track points $dy = 0.6$ m, the number of the track points $n = 168$, and the length of the track $L = 100$ m. As the homogeneous soil has only a weak attenuation with distance, the train passage does not start with a zero amplitude. To avoid any boundary effect, a Hanning window

$$h_H(y) = \cos^2\left(\frac{\pi y}{L}\right) \quad (25)$$

is used.

4. Theoretical Results

The results of this section are based on a standard ballast track. The relevant parameters are the bending stiffness of the rail $EI = 6.4 \text{ Nm}^2$, the mass per length of the rail $m' = 60 \text{ kg/m}$, the stiffness of the rail pad $k_R = 3 \cdot 10^8 \text{ N/m}$ or infinite, the sleeper mass $m_S = 340 \text{ kg}$, the sleeper distance $d = 0.6 \text{ m}$, the ballast height $h_B = 0.3 \text{ m}$, and the shear wave velocity of the soil $v_S = 200 \text{ m/s}$ and the ballast $v_S = 300 \text{ m/s}$. The standard vehicle parameters of interest are the wheelset mass $m_W = 1500 \text{ kg}$ and the axle distance within a bogie $2l_B = 2.5 \text{ m}$. The standard train has 40 axles with a static axle load of $F_0 = 100 \text{ kN}$ on a train length of 250 m.

4.1. Transfer Functions of the Vehicle-Track Interaction

First, the most important vehicle-track-soil transfer function $F_S/s = H_T H_V$ is presented for the variation of some vehicle and track parameters. The vehicle-track-soil transfer function is strongly influenced by the unsprung mass of the vehicle, the wheelset mass (Figure 4a). The dynamic axle loads are proportional to the wheelset mass for frequencies up to 64 Hz. For this frequency range, the transfer function increases strongly with $F_S/s \sim f^2$. If soft under-sleeper pads are added to the track (Figure 4b), resonances can be seen at frequencies between 16 and 64 Hz. Above these resonance frequencies, the dynamic axle-loads can be reduced to less than one-tenth of the values of a standard ballast track. Vehicle-track resonances, however, do not occur for the standard ballast track in the frequency range of interest.

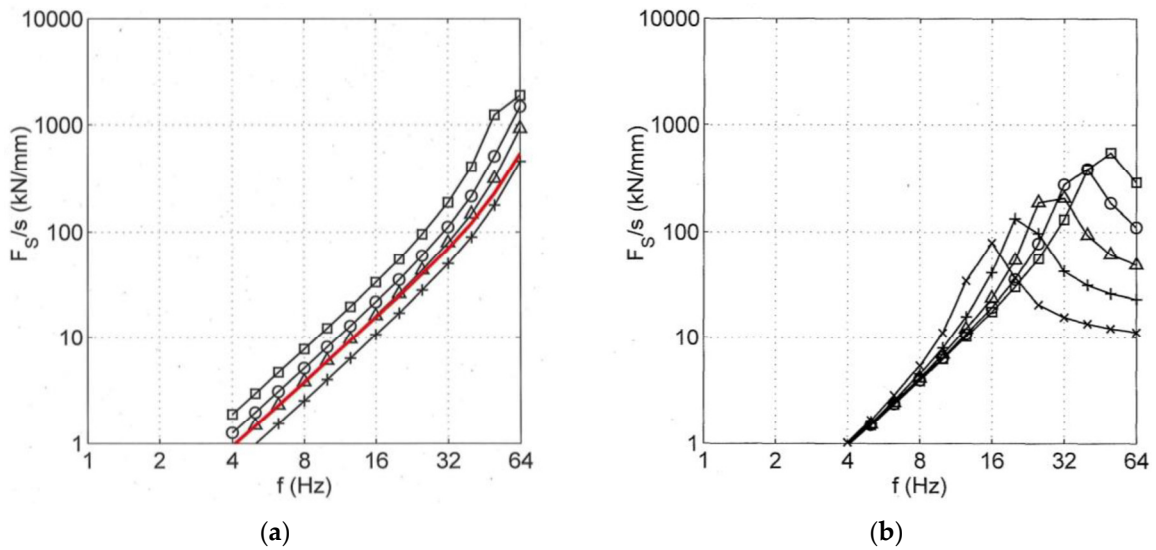


Figure 4. Transfer functions of vehicle–track interaction (dynamic axle loads due to irregularities) (a) for different wheelset masses $m_W = + 1000, \Delta 1500, \circ 2000,$ and $\square 3000$ kg, $- 1500$ kg with $H_T(f) = 1$, and (b) for different under-sleeper pads with stiffness of $k_p = \times 10, + 20, \Delta 40, \circ 80,$ and $\square 160 \times 10^6$ N/m.

4.2. Transfer Functions of the Track Filtering

The track filtering functions for the geometric and stiffness-induced track support irregularities are shown in Figure 5. Figure 5a shows that the low-frequency geometric track support irregularity s_S is passed directly through the track to give the rail irregularity s_R , yielding a transfer value of $s_R/s_S = 1$. Frequencies higher than 12 Hz (in case of a standard ballast track and train speed of $v_T = 160$ km/h) are reduced considerably because of a strong cut-off effect. The ballast tracks with soft sleeper pads have lower cut-off frequencies down to 8 Hz and, therefore, a stronger track filtering effect with lower effective track irregularities.

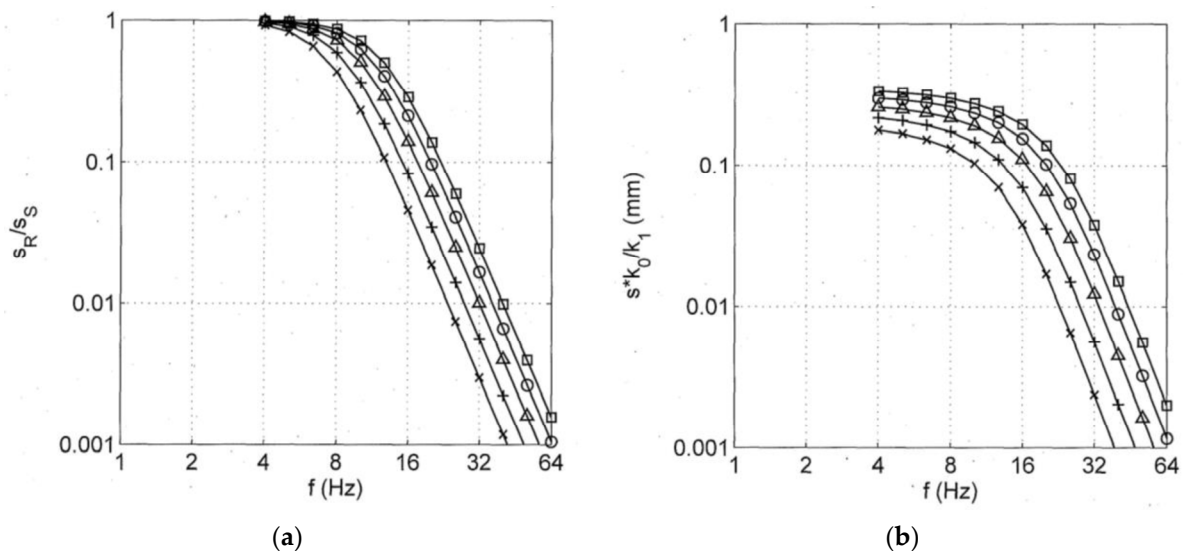


Figure 5. Transfer functions for the track filtering (a) of geometric track bed errors, and (b) of a stiffness variation, ballast tracks with different under-sleeper pads with stiffness of $k_p = \times 10, + 20, \Delta 40, \circ 80,$ and $\square 160 \times 10^6$ N/m.

Similar observations are made for the stiffness-induced track support irregularities in Figure 5b, but the cut-off frequencies are somewhat higher, between 12 and 20 Hz, and the

low-frequency transfer values depend on the stiffness of the track. The low-frequency force amplitudes are smaller for the softer sleeper pads.

4.3. Quasi-Static Ground Response

First, the effect of the axle pulses on a regular track support is examined. A train with speed of 160 km/h and three homogeneous soils with shear wave velocities of $v_s = 150, 200$ and 300 m/s are considered. The train passage is presented as one-third of the octave band spectra of the particle velocity for the distances $x = 3, 5,$ and 10 m in Figure 6a–c. The moving static loads induce very low-frequency vibrations in the neighbourhood of the railway line. The main amplitudes of this quasi-static solution are below 12 Hz at 3 m, below 6 Hz at 5 m, and below 3 Hz at 10 m. The spectra strongly decrease with frequency and with distance. This means that the regular response to the static loads is limited to the low-frequency near field of the track (see also [36–38]), except for trans-Rayleigh-trains in very soft soils [18]. The quasi-static ground vibration amplitudes are also reduced in a stiffer soil (Figure 6c). The typical spectra of the different distances can be used to easily identify the quasi-static component in the following calculations. In measurements, there may be some additional low-frequency maxima and minima due to special train configurations. Note that the low-frequency quasi-static solution was calculated from axle impulses of higher frequency content. The result is very similar to a calculation based on the static transfer function of the soil [37]. Obviously, the higher impulse frequencies, which come from different track points, perfectly cancel each other.

4.4. The Effect of Axle Pulses on a Randomly Varying Track Support Stiffness

Next, the train was run over an irregular track support and the ground vibration spectra are shown in Figure 6d–f. Once again, the passage of static loads generates the quasi-static response of the soil. The typical spectra can be observed below 8 Hz. For frequencies above 8 Hz, a big difference between the regular and irregular track support is obvious. Whereas the quasi-static component tends to zero, the varying track support stiffness generates a new ground vibration component with considerable amplitudes. The low-frequency quasi-static and the mid-frequency response are clearly separated by a minimum at around 8 Hz. There is a second minimum at 25 or 32 Hz, so that the mid-frequency ground vibration component can be identified by a typical maximum region between these minima. This characteristic is related to the axle-sequence spectrum $X_A(f)$ of a bogie. The mid-frequency component also has a completely different attenuation with distance. In contrast to the strong attenuation of the quasi-static component, the mid-frequency part has a rather weak attenuation.

The mid-frequency stochastic ground vibration component is generated as follows. The static axle load runs over different excitation points of the track that have different stiffnesses. If the track is stiffer, the impulse is shorter and has a wider bandwidth. If the track is softer, the impulse is longer and the bandwidth is narrower. Therefore, low frequencies of the impulse are similar for all excitation points, but the amplitudes around the bandwidth vary considerably. The impulses from neighbouring excitation points cannot perfectly cancel each other. The remainder of the superposition constitutes the new mid-frequency ground vibration component (which is called “the scattered axle pulses”).

Figure 7a–d shows the one-third octave band spectra for $q = 3, 10, 30$ and 50% variation of the track support stiffness. The mid-frequency range strongly increases with the percentage of the stiffness variation. At the end for 50% variation, the mid-frequency amplitudes are as high as for the nearest quasi-static response. The stochastic mid-frequency component is only moderately higher for a softer soil (Figure 6d). Another variation in Figure 7d–f shows the influence of the track stiffness on the mid-frequency component. The bending stiffness EI of the track is increased from the rail to $10 EI$ and $100 EI$, where $100 EI$ is approximately the stiffness of a 0.5 m thick concrete plate. The mid-frequency amplitudes are clearly reduced by a stiff plate, to less than one-tenth. The stiff plate results in a wider distribution of the static load along the track. This means a smoother impulse, which has

lower frequencies and lower amplitudes. Thus, a new ground vibration component was found, but also a possible mitigation strategy for this component.

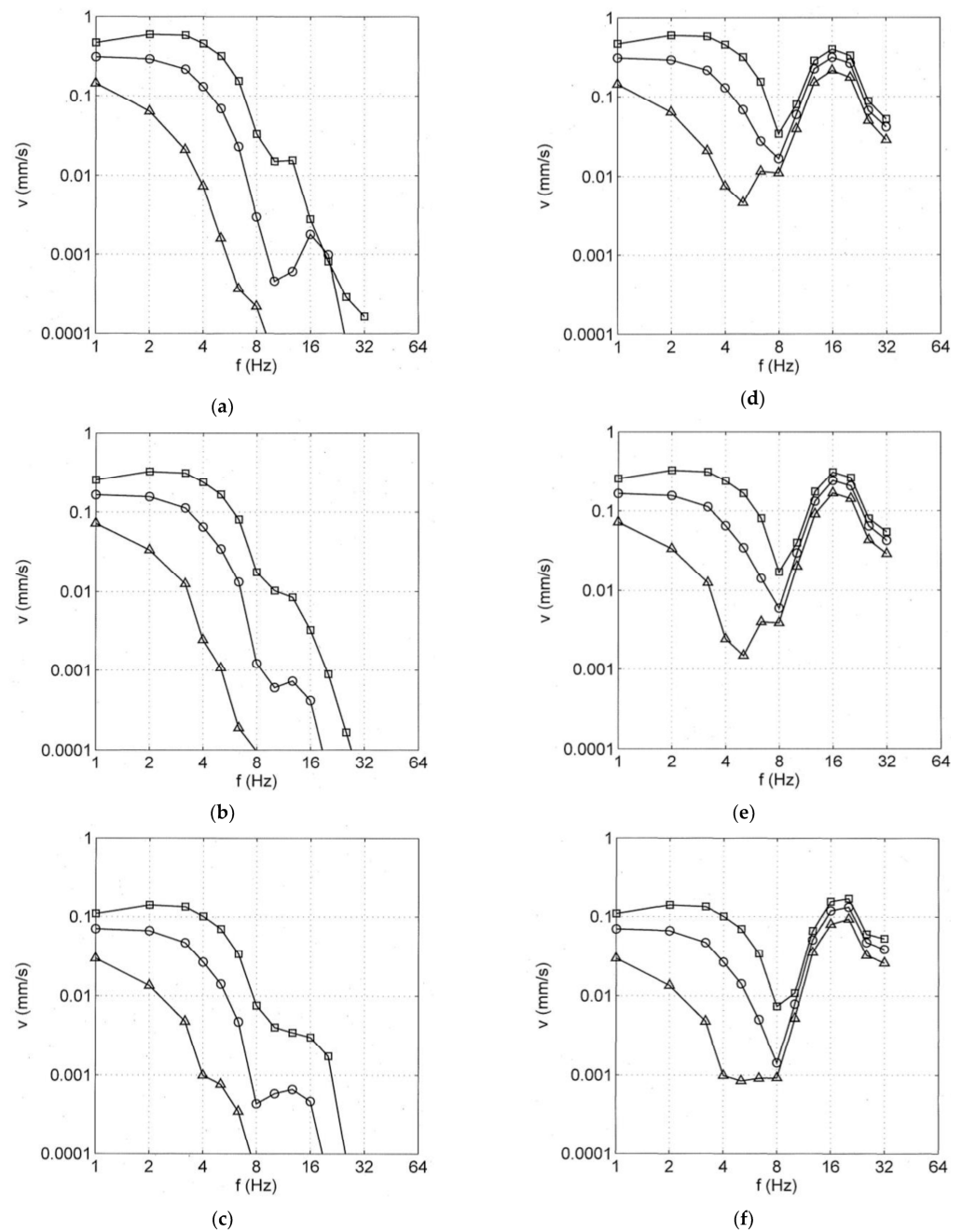


Figure 6. Train passage with $v_T = 160$ km/h over a regular (a,c,e) and an irregular ballast track (b,d,f), $q = 50\%$, different soils with $v_S =$ (a,b) 150, (c,d) 200, (e,f) 300 m/s, one-third of the octave band spectrum at distances $x = \square 3, \circ 5, \Delta 10$ m.

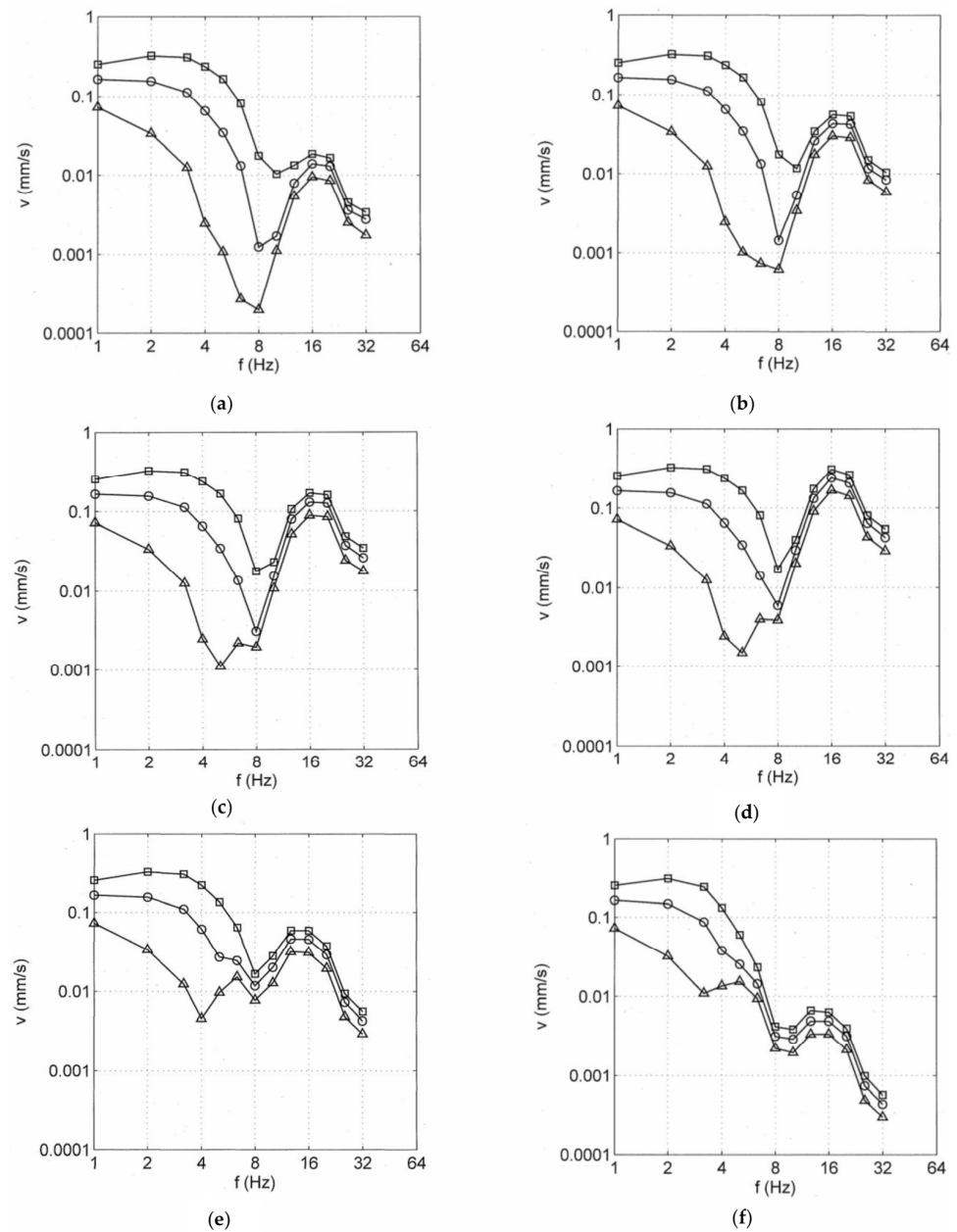


Figure 7. Train passage with $v_T = 160$ km/h over an irregular track and a soil with $v_S = 200$ m/s, irregularity $q =$ (a) 3%, (b) 10%, (c) 30%, (d–f) 50%, track stiffness (a–d) EI ballast track, (e) 10 EI, (f) 100 EI slab track, one-third of the octave band spectrum at distances $x = \square$ 3, \circ 5, Δ 10 m.

5. Calculated and Measured Results at a Specific Site

At a site near Würzburg, simultaneous vibration measurements of the train, the track and the soil were performed at three different track sections for different train speeds [4]. The axle-box measurements and the hammer and train-induced ground vibrations near the ballast track are used here to compare theoretical predictions with measurements.

5.1. Wheelset Accelerations from Axle-Box Measurements and Corresponding Irregularities and Forces

First, the measured axle-box accelerations are shown in Figure 8a for five train speeds. The spectra are almost constant with frequency. The only exception is for the lowest speed of 63 km/h where an increase at 32 Hz can be related to the sleeper passage excitation. The accelerations are strongly increasing with train speed, and an amplitude factor of 10 is observed for train speeds between 63 and 160 km/h. Four different axle boxes were

measured and all four measurement points give very similar results. Only the out of roundness at 8, 10, 12, or 16 Hz is specific for each wheel.

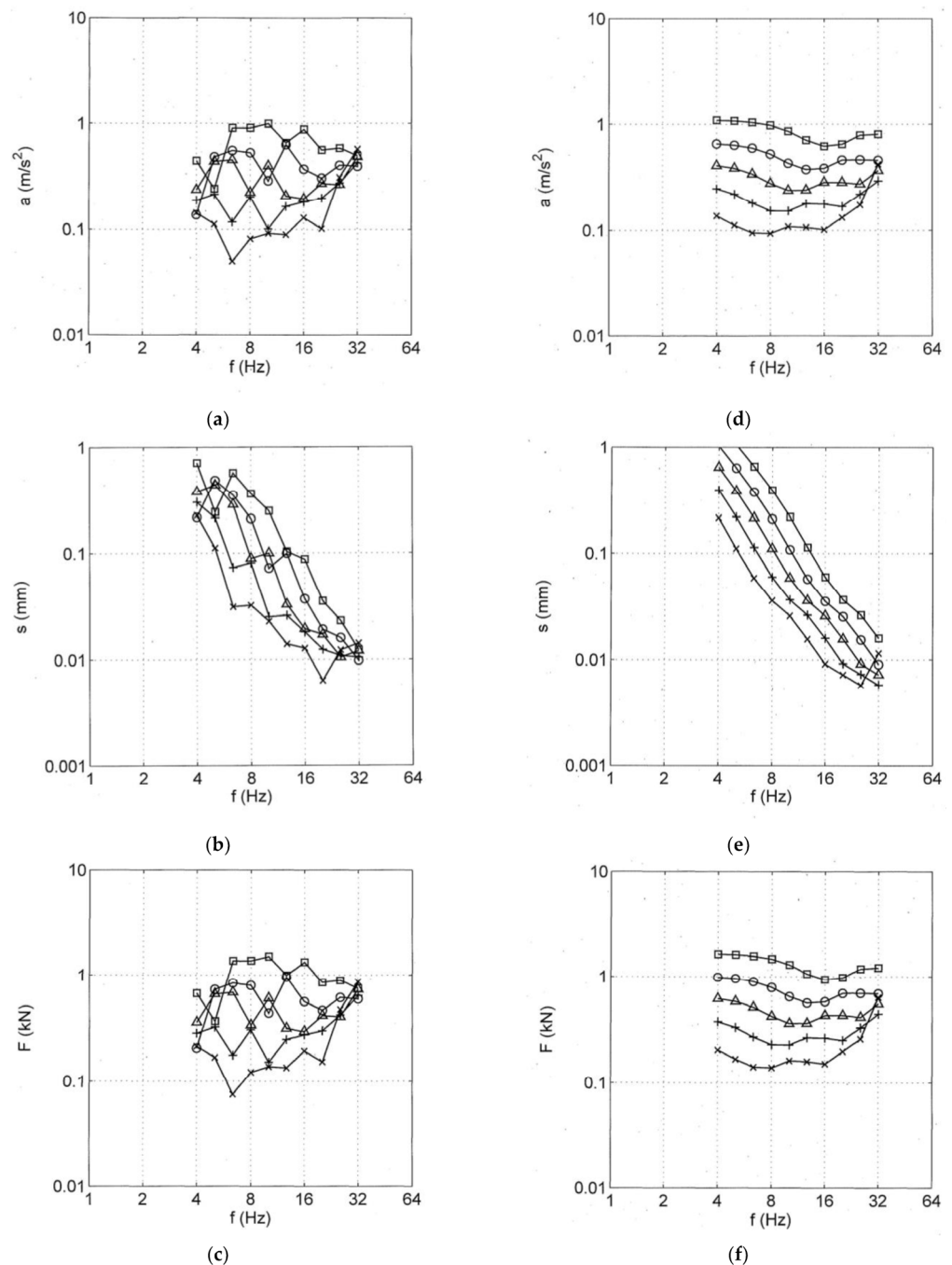


Figure 8. Measured (a–c) and calculated (d–f) vehicle–track interactions at site W for train speeds $v_T = \square$ 160, \circ 125, Δ 100, $+$ 80, and \times 63 km/h; wheelset acceleration (a,d), effective irregularities (b,e), dynamic axle loads (c,f).

The measured wheelset accelerations a_W are divided by ω^2 to yield displacements (Figure 8b). These wheel displacements are the same as the effective irregularities s in this frequency range; see [31]. The irregularities are strongly decreasing with frequency. The accelerations a_W multiplied by the wheelset mass of $m_W = 1500$ kg are almost identical to the excitation forces F acting on the track (Figure 8c), with small deviations at low frequencies due to bogie contributions [31]). Therefore, the forces are almost constant with frequency and strongly increasing with train speed in the same way as the accelerations.

Corresponding results are calculated with the transfer functions of Section 3.2 and the following irregularities s_S of the subground and s_W the combined unevenness of wheel and rail:

$$\begin{aligned} s_S &= s_{S1}(\lambda/\lambda_1)^2 \text{ with } s_{S1} = 0.02 \text{ mm at } \lambda_1 = 1.2 \text{ m} \\ s_W &= s_{W1}(\lambda/\lambda_1) \text{ with } s_{W1} = 0.01 \text{ mm at } \lambda_1 = 1.2 \text{ m} \end{aligned} \quad (26)$$

The stiffness variation is assumed to be constant at $k_1/k_0 = 20\%$, and the stiffness variation by the sleeper passage is included as an effective irregularity of $s_D = 0.012$ mm. The resulting effective irregularity at rail level is shown in Figure 8e. For the train speed of 100 km/h (curve Δ), the following components can be observed. At low frequencies, the geometric track support irregularities dominate, but also strongly decrease with $s_R \sim f^{-2}$. The transfer function H_{sT} for the geometrical track support irregularity has a cut-off at about 8 Hz and, therefore, the effective irregularity s^* from the support stiffness variation dominates at about 12 Hz. This component is initially constant with frequency and the cut-off of the corresponding transfer function H_{kT} is at about 20 Hz, from where the stiffness component also decreases until the wheel and track unevenness s_W is dominant at 25 Hz.

In the next step, the decreasing irregularities have to be multiplied by the increasing vehicle-track transfer functions (6) and (7). The resulting axle-load spectra in Figure 8f are almost constant with frequency. The amplitudes increase with increasing train speed as $F \sim v_T^2$. The dynamic load is about $F \approx 0.4$ kN for 100 km/h and reaches $F \approx 1.0$ kN for 160 km/h.

The measurements and calculations of the train-track interaction are in good agreement in all details: the irregularities are strongly decreasing with frequency, and the accelerations and forces are constant in frequency and strongly increasing with train speed $A \sim v_T^2$, and have the same amplitude of 1.0 kN for 160 km/h.

5.2. Measured and Calculated Transfer Functions of the Soil

The transfer functions of the soil at this site were measured by hammer impacts and sensor distances between 3 and 30 m (Figure 9a). A soil model was fitted to these transfer functions, which consists of a layer of height $h = 11$ m, a shear wave velocity $v_{S1} = 270$ m/s and an underlying half-space of $v_{S2} = 1000$ m/s. The theoretical transfer functions of this layered situation are presented in Figure 9b, which show all the same characteristics as the measured transfer functions. The low-frequency amplitudes are small because of the stiff half-space, whereas the high frequencies have the greater amplitudes of the softer layer. Between these two different amplitude ranges, a strong increase in amplitudes can be found, which is followed by a moderate resonance at 12.5 Hz.

The transfer functions in Figure 9a,b hold for a point load. A number of point loads of a 1 kN amplitude per axle and one-third octave band were superposed stochastically to obtain the transfer function for a train load (the response to a standard train load, Figure 9c). The characteristics are the same as for the point load. The near field has almost the same amplitude, whereas the far field of the train load has higher amplitudes. This leads to a weaker attenuation with distance and a narrower band of transfer functions.

Another representation is given for the results at a 30 m distance. Figure 9d shows the spectra for different train speeds v_T , which are calculated by different dynamic loads of $F = 0.155$ to 1.0 kN per axle and one-third octave band. The curves are regularly shifted vertically upwards proportional to the dynamic axle load.

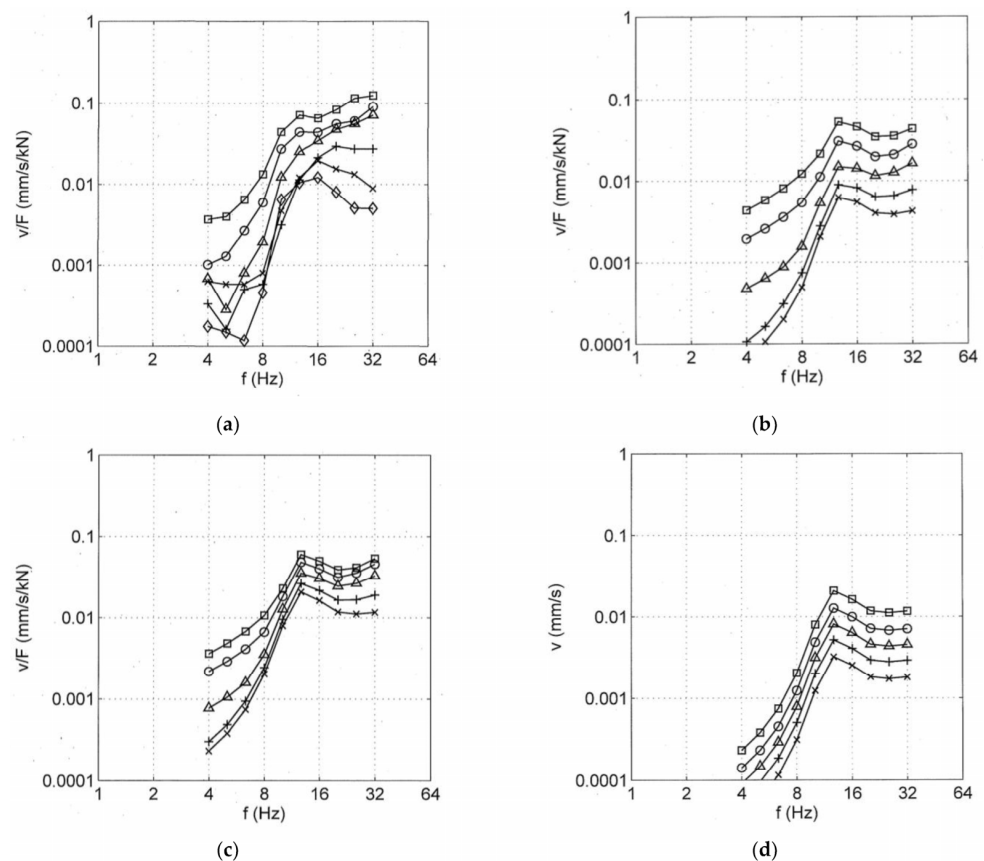


Figure 9. Transfer functions for the soil at site W, distances $x = \square 3, \circ 5, \Delta 10, + 20, \times 30$ m, (a) measured from hammer impact, (b) calculated for a point load, (c) calculated for a standard train load; (d) response to constant train loads between 0.15 and 1 kN per one-third octave band representing train speeds of $v_T = \square 160, \circ 125, \Delta 100, + 80, \times 63$ km/h.

5.3. Ground Vibrations from Static or Dynamic Axle Loads and from Measurement

Now the ground vibrations from train passages are predicted and compared with the measurements. The response at different distances from the track (for a train speed of 160 km/h) and the response for different train speeds (at a distance of 30 m) are shown in Figure 10. Theoretical responses are shown for the dynamic loads from irregularities in Figure 10a,b and for the static loads on a varying track support. In addition to the transfer functions H_S of the layered soil, the axle sequence X_A Equation (22) of the bogies is included in both cases.

The wave field for the dynamic loads (Figure 10a) is very similar to the transfer functions in Figure 9c, as the dynamic loads are (almost) constant and at 1 kN for 160 km/h. In addition to the characteristics of the layered soil, the maximum at 12.5 Hz is increased slightly because of the axle sequence spectrum. The different train speeds (Figure 10b) have different axle sequence spectra, so that the regular pattern of Figure 9d is lost. The strict order of the train speeds can only be found at the highest frequencies. A clear maximum occurs only for 125 and 160 km/h.

The measured train-induced wave field (Figure 10c) shows the small low-frequency amplitudes of the deeper stiff soil and the strong increase at about 10 Hz. The maximum at 12.5 Hz is more pronounced than for the transfer functions (Figure 9c) as the curves of all distances come close together. The high-frequency amplitudes are approximately those of the upper layer. The curves of different train speeds (Figure 10d) show clearly elevated responses for 125 and 160 km/h, whereas the train speeds below 100 km/h induce only smaller ground vibrations. The ground vibrations from dynamic loads in Figure 10a

and b are clearly smaller than (less than half) the ground vibration from measurements in Figure 10c,d.

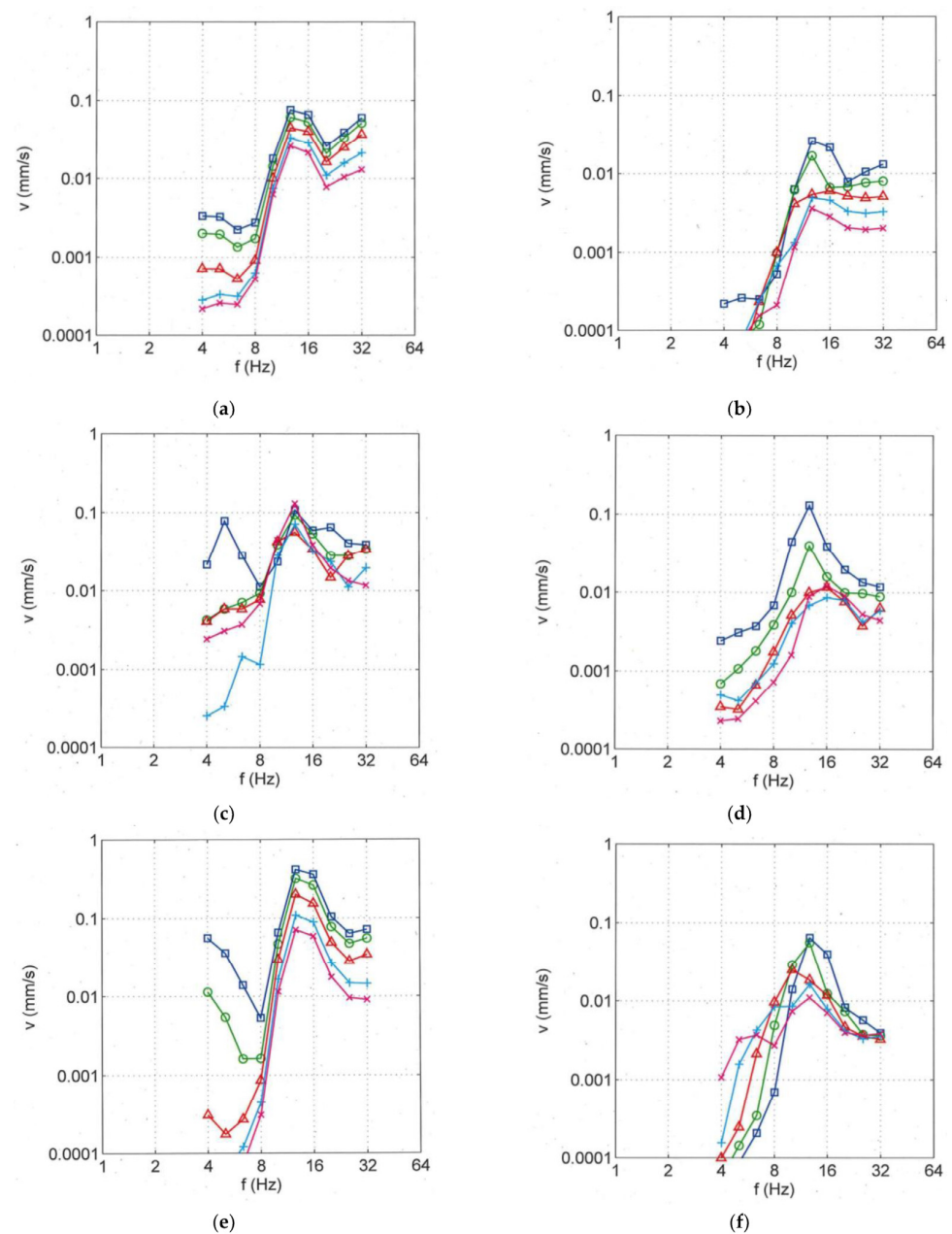


Figure 10. Comparison of measured and calculated ground vibrations; wavefield at distances $x = \square 3, \circ 5, \Delta 10, + 20, \times 30$ m for the maximum train speed of 160 km/h (a,c,e), and for different train speeds of $v_T = \square 160, \circ 125, \Delta 100, + 80, \times 63$ km/h at a distance of 30 m (b,d,f), calculated with geometric track irregularities (a,b), measured at site W (c,d), and calculated by a varying track support stiffness (e,f).

The ground vibrations from the static loads are presented in Figure 10e,f. In the near field, the quasi-static component can be found between 4 and 6 Hz. All other amplitudes are the result of the varying track support stiffness. The maxima at 12.5 Hz are increased by the pulses of the static axle loads, and they are much higher than for the dynamic loads in Figure 10a,b. The minima are almost at the same frequencies (8 Hz and 20/25 Hz) for the static loads, the dynamic loads and the measurements. The minima are strongest for the static pulse loads, which have an extra reduction in addition to the minima from the axle sequence and the low frequency reduction in the layering. The maximum, on the other

hand, is increased by the static pulse loads in addition to the nearby (moderate) maxima of the axle sequence and the resonance of the layering. Because of these effects, the static loads yield the highest near-field amplitudes at 12.5 Hz, and at 30 m, they generate a maximum (Figure 10f), which is clearly higher than the maximum of the dynamic loads (Figure 10b) and nearly reaches the amplitude of the measurements (Figure 10d).

These measured and calculated results show that the elevated mid-frequency vibrations can be better explained by the randomly varying track support than by the dynamic loads from the irregularities. The importance of the axle pulses on an irregular track and soil (the scattering of axle pulses) for the ground vibration near railway lines was indicated by more experimental results of BAM [31,37,39], and in [40] measurements of other researchers were re-sampled and collected from, for example, [14,17,19,41,42].

6. Conclusions

The excitation of ground vibrations by different irregularities of the railway track was analysed, considering the widely used geometric irregularities at the wheel–rail contact, stiffness irregularities, irregularities from different track positions and irregularities in the wave propagation. Formulas were given in the frequency-wavenumber domain, and example transfer functions (the force on the soil related to the specific irregularity) were calculated. The transfer functions show the increasing influence of the wheelset mass and the reducing influence of soft track elements (e.g., sleeper pads). The latter yield cut-off frequencies of 8 to 16 Hz and resonance frequencies of 16 to 50 Hz. Whereas most irregularities generate dynamic axle loads, static (gravity-induced) loads of the vehicle have some special effects. The static loads are moving constant loads, which were calculated as the very low-frequency quasi-static component of the near-field ground vibration. In the case where the track support stiffness varies randomly along the track, the results for the moving constant loads were calculated by the frequency-domain superposition of axle pulses and a stochastic simulation. This computation yields, in addition to the regular quasi-static component, a strong stochastic mid-frequency component because of the “scatter” of the axle pulses.

Experimental results of simultaneous vehicle, track and soil measurements were presented and compared with the theoretical results for the dynamic and static loads. Effective track irregularities, dynamic axle loads and ground vibration at different distances and for different train speeds were analysed. It was found that the dynamic loads that are evaluated from the measured axle-box accelerations are not great enough to generate the measured ground vibrations. The stochastic component of the moving static load, however, can generate the higher measured ground vibration amplitudes. This indicates that a static load moving over a varying track support stiffness can produce an important ground vibration component by the scatter of axle pulses.

Funding: This research received no external funding.

Institutional Review Board Statement: Not applicable.

Informed Consent Statement: Not applicable.

Data Availability Statement: The data of this study are available on request from the author.

Acknowledgments: The ground vibration measurements have been done in good cooperation with S. Said and W. Schmid.

Conflicts of Interest: The author declares no conflict of interest.

Abbreviations

a	amplitude vector
<i>b</i>	width of the track
C	damping matrix of the multi-beam track model
<i>df</i>	frequency step
<i>df_T</i>	one-third octave frequency band
<i>dt</i>	time step
<i>dy</i>	load step
e₁	base vector (top of the track)
e_n	base vector (bottom of the track)
<i>El_j</i>	bending stiffness of track beam <i>j</i>
EI	matrix of bending stiffnesses
<i>f</i>	frequency
<i>f_T</i>	one-third octave frequency
<i>f₀</i>	cut-off frequency of the track
F	force, axle load
F'	force per track length
<i>F₀</i>	static axle load
<i>F_S</i>	force on the soil
<i>F_T</i>	force on the track
F'_T	force vector (forces on different track beams)
<i>h</i>	height of the soil layer
<i>H_{zz}</i>	transfer function of the homogeneous half-space in wavenumber domain
<i>H_H</i>	transfer function of the homogeneous half-space in space domain
<i>H_F</i>	filter function of the track
<i>H_{kT}</i>	transfer function for the stiffness irregularity
<i>H_{sT}</i>	transfer function for the stiffness variation of the track support
<i>H_S</i>	transfer function of the soil for a point load
<i>H_{SS}</i>	transfer function of the soil for a strip load
<i>H_T</i>	force transfer of the track
<i>H_V</i>	vehicle-track transfer function
<i>H_V*</i>	vehicle-track transfer function for stiffness-induced irregularities
<i>k_P</i>	stiffness of the sleeper pad
<i>k_R</i>	stiffness of the rail pad
<i>k_S</i>	dynamic stiffness of the track support
<i>k_S*</i>	dynamic stiffness of the Winkler support
<i>k₀</i>	average static stiffness of the track support
<i>k₁</i>	stiffness variation of the track support
<i>K_T</i>	dynamic stiffness of the track at the wheel-rail contact point
<i>K_V</i>	dynamic stiffness of the vehicle at the wheel-rail contact point
K₀	average static stiffness of the track
K₁	stiffness variation of the track
K	stiffness matrix of the multi-beam track model
K_S	dynamic stiffness matrix of the soil
K_T	stiffness matrix of the track
K_{TS}	stiffness matrix of the track-soil system
<i>l_B</i>	half the distance between two axles in a bogie
<i>m_W</i>	mass of the wheelset
<i>m'_j</i>	mass per length of track beam <i>j</i>
M	mass matrix
<i>n</i>	number of loading points
<i>n_B</i>	number of bogies in a train
<i>p</i>	stress distribution across the track
<i>q</i>	percentage of the variation in the support stiffness
<i>s</i>	(geometric) irregularity

s^*	equivalent irregularity
s_D	equivalent displacement variation due to sleeper distance excitation
s_R	irregularity at rail level
s_S	irregularity at the track support
s_W	irregularity of the wheel
t	time
t_j	loading time of position j
\mathbf{t}	stress vector
\mathbf{u}	displacement vector
u_R	displacement of the rail
u_S	displacement of the track support
v	particle velocity (of the soil)
v_S	shear wave velocity of the soil
v_{S1}	shear wave velocity of the layer
v_{S2}	shear wave velocity of underlying half-space
v_T	train speed
X	axle-sequence spectrum of the train
X_A	axle-sequence spectrum for two axles of a bogie
x	coordinate normal to the track
y	coordinate along the track
y_j	coordinate of the loading point j
δ	Dirac function
λ	Wavelength
ξ	Wavenumber
ξ_x	wavenumber normal to the track
ξ_y	wavenumber along the track
ξ_V	wavenumber of the stiffness variation
ω	circular frequency

Appendix A. Frequency-Wavenumber Domain Methods and Their Approximation for Dynamic Track and Soil Behaviour

The dynamic behaviour of a layered soil is algebraically calculated in the frequency-wavenumber domain. The resulting vertical compliance H_{zz} of the soil surface is used twofold. The compliance for a point-load (the wave field as a function of distance r and ω) is established by the integral [35]

$$H_S(r, \omega) = \frac{u(r, \omega)}{F(\omega)} = \frac{1}{2\pi} \int_0^\infty H_{zz}(\xi, \omega) J_0(\xi r) \xi d\xi \quad (\text{A1})$$

where J_0 is the Bessel function. The transfer function $H_S(\omega, r)$ of the wave propagation through a layered soil can be approximated by the transfer function $H_H(\omega, r, v_S)$ of the homogeneous soil and the frequency-dependent wave velocity $v_S(\omega)$ (the dispersion of the soil) [40]. Figure A1 shows the good agreement between the exact and approximate transfer functions for the wave propagation in a soft layer on a stiffer half-space.

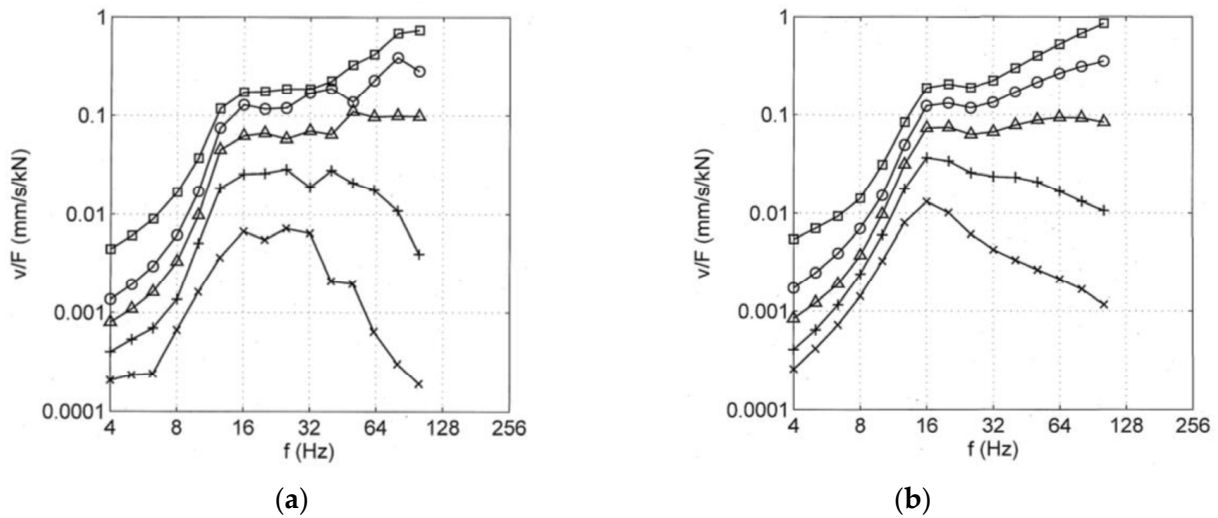


Figure A1. Transfer function of a soil with $v_{S1} = 125$ m/s, $v_{S2} = 350$ m/s, $h = 4$ m, $D = 2.5\%$ at distances $x = \square 4, \circ 8, \Delta 16, + 32, \times 64$ m, (a) exact, (b) approximated solution.

For a harmonic strip wave excitation along the railway track (y-direction)

$$\mathbf{t}(x, y) = \mathbf{a} \exp(i\zeta_y y + i\omega t) \quad \text{for } |x| < b/2 \tag{A2}$$

the displacements across the track–soil interface (x-direction)

$$u_S(x, \zeta_y, \omega) = \frac{F'(\zeta_y, \omega)}{2\pi} \int_{-\infty}^{+\infty} H_{zz}(\sqrt{\zeta_x^2 + \zeta_y^2}, \omega) p(\zeta_x) \exp(i\zeta_x x) d\zeta_x \tag{A3}$$

are calculated, where the wavenumber transform of the uniform load distribution across the track width b

$$p(\zeta_x) = \frac{\sin \zeta_x b/2}{\zeta_x b/2} \tag{A4}$$

is used. Moreover, the average displacement

$$\bar{u}_S(\zeta_y, \omega) = \frac{1}{b} \int_{-b/2}^{+b/2} u_S(x, \zeta_y, \omega) \exp(i\zeta_x x) dx \tag{A5}$$

across the track is calculated. Finally, the soil compliance for a strip load

$$H_{SS}(\zeta_y, \omega) = \frac{\bar{u}_S(\zeta_y, \omega)}{F'(\zeta_y, \omega)} = \frac{1}{2\pi} \int_{-\infty}^{+\infty} H_{zz}(\sqrt{\zeta_x^2 + \zeta_y^2}, \omega) p^2(\zeta_x) d\zeta_x \tag{A6}$$

is established. The inverse

$$k_S(\zeta_y, \omega) = \frac{1}{H_{SS}(\zeta_y, \omega)} \tag{A7}$$

is the soil stiffness, which is used for coupling the soil with the track.

The stiffness of the soil can be approximated by a Winkler soil as

$$k_S(\zeta_y, \omega) \approx k_S^*(\omega) = k_W + i\omega c_W \tag{A8}$$

Figure A2 shows the comparison of the track stiffness calculated by the wavenumber method and by the Winkler approximation. The agreement between these two results and the results of the combined boundary-element/finite-element method [32] is good.

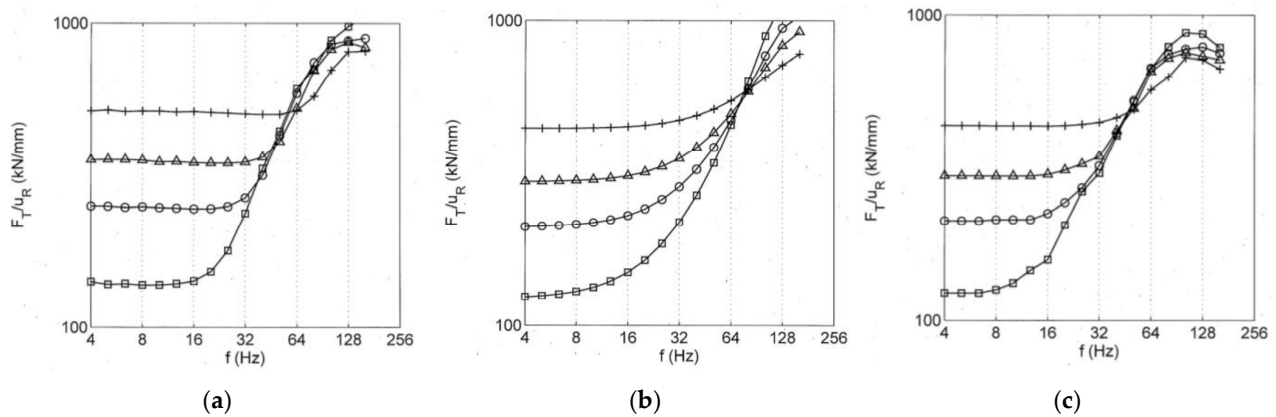


Figure A2. Dynamic stiffness of standard ballast track on soils with $v_s = \square 100, \circ 150, \Delta 200, + 300$ m/s, (a) wavenumber domain method with continuous soil, (b) with approximated Winkler soil, (c) boundary-element/finite-element method.

References

- Berawi, A. Improving Railway Track Maintenance Using Power Spectral Density (PSD). Ph.D. Thesis, University of Porto, Porto, Portugal, 2013.
- Hamid, A.; Rasmussen, K.; Baluja, M.; Yang, T. *Analytical Description of Track Geometry Variations*; Report for Federal Railroad Administration; ENSCO Inc.: Springfield, IL, USA, 1983.
- Esveld, C. *Modern Railway Track*; MRT-Productions: Duisburg, Germany, 1989.
- Auersch, L. Simultaneous measurements of the vehicle, track, and soil vibrations at a surface, bridge, and tunnel railway line. *Shock. Vib.* **2017**, *2017*, 1959286. [\[CrossRef\]](#)
- Takemiya, H. Ground vibrations alongside tracks induced by high-speed trains: Prediction and mitigation. In *Noise and Vibration from High-Speed Trains*; Krylov, V., Ed.; Thomas Telford: London, UK, 2001; pp. 347–391.
- Sheng, X.; Jones, C.; Thompson, D. A theoretical model for ground vibration from trains generated by vertical track irregularities. *J. Sound Vib.* **2004**, *272*, 937–965. [\[CrossRef\]](#)
- Lombaert, G.; Degrande, G.; Kogut, J.; François, S. The experimental validation of a numerical model for the prediction of railway induced vibrations. *J. Sound Vib.* **2006**, *297*, 512–535. [\[CrossRef\]](#)
- Maldonado, M. Vibrations Dues au Passage d'un Tramway—Mesures Expérimentales et Simulations Numériques. Ph.D. Thesis, Ecole Centrale de Nantes, Nantes, France, 2009.
- Ju, S.; Lin, H. Experimentally investigating finite element accuracy for ground vibrations induced by high-speed trains. *Eng. Struct.* **2008**, *30*, 733–746. [\[CrossRef\]](#)
- Kouroussis, G. Modélisation des Effets Vibratoires du Traffic Ferroviaire sur L'environnement. Ph.D. Thesis, University of Mons, Mons, Belgium, 2009.
- Connolly, D. Ground Borne Vibrations from High-Speed Trains. Ph.D. Thesis, University of Edinburgh, Edinburgh, UK, 2013.
- Ekevid, T.; Wiberg, N. Wave propagation related to high-speed train: A scaled boundary FE-approach for unbounded domains. *Comput. Methods Appl. Mech. Eng.* **2002**, *191*, 3947–3964. [\[CrossRef\]](#)
- Galvin, P.; Dominguez, J. Experimental and numerical analyses of vibrations induced by high-speed trains on the Cordoba-Malaga line. *Soil Dyn. Earthq. Eng.* **2009**, *29*, 641–657. [\[CrossRef\]](#)
- Romero, A. Predicción, Medida Experimental y Evaluación de las Vibraciones Producidas por el Tráfico Ferroviario. Ph.D. Thesis, University of Sevilla, Sevilla, Spain, 2012.
- Yang, Y.; Hung, H. A 2.5D finite/infinite finite element approach for modelling viscoelastic bodies subjected to moving loads. *Int. J. Numer. Methods Eng.* **2001**, *51*, 1317–1336. [\[CrossRef\]](#)
- Galvin, P.; Francois, S.; Schevenels, M.; Bongini, E.; Degrande, G.; Lombaert, G. A 2.5D coupled FE-BE model for the prediction of railway induced vibrations. *Soil Dyn. Earthq. Eng.* **2010**, *30*, 1500–1512. [\[CrossRef\]](#)
- Alves Costa, P. Vibrações do Sistema Via-Maçiço Induzidas por Tráfego Ferroviário—Modelação Numérica e Validação Experimental. Ph.D. Thesis, University of Porto, Porto, Portugal, 2011.
- Krylov, V. Ground vibration boom from high-speed trains: Prediction and reality. *Acoust. Bull.* **1998**, *23*, 15–22.
- Triepaischajonsak, N.; Thompson, D.; Jones, C.; Ryue, J.; Priest, J. Ground vibration from trains: Experimental parameter characterisation and validation of a numerical model. *Rail Rapid Transp.* **2011**, *225*, 140–153. [\[CrossRef\]](#)
- Auersch, L. Theoretical and experimental excitation force spectra for railway induced ground vibration—Vehicle-track soil interaction, irregularities and soil measurements. *Veh. Syst. Dyn.* **2010**, *48*, 235–261. [\[CrossRef\]](#)
- Verheijen, E. A survey on roughness measurement. *J. Sound Vib.* **2006**, *293*, 784–794. [\[CrossRef\]](#)
- Johansson, A. Out-of-Round Railway Wheels—Literature Survey, Field Tests and Numerical Simulations. Ph.D. Thesis, University of Göteborg, Gothenburg, Sweden, 2003.

23. Hunt, H. Types of rail roughness and the selection of vibration isolation measures. In *Noise and Vibration Mitigation for Rail Transportation Systems; Notes on Numerical Fluid Mechanics and Multidisciplinary Design*; Springer: Berlin/Heidelberg, Germany, 2008; Volume 99, pp. 341–347.
24. Auersch, L. Excitation of ground vibration due to the passage of trains over a track with trackbed irregularities and a varying support stiffness. *Veh. Syst. Dyn.* **2015**, *53*, 1–29. [[CrossRef](#)]
25. Verachtert, R.; Hunt, H.; Hussein, M.; Degrande, G. Changes of perceived unevenness by in-track vibration countermeasures in slab track. *Eur. J. Mech. A/Solids* **2017**, *65*, 40–58. [[CrossRef](#)]
26. Auersch, L. Parametric excitation of rail-wheel-system: Calculation of vehicle–track–subsoil-dynamics and experimental results of the high-speed train Intercity experimental. *Arch. Appl. Mech.* **1990**, *60*, 141–156. (In German)
27. Nielsen, J.; Igeland, A. Vertical dynamic interaction between train and track—Influence of wheel and track imperfections. *J. Sound Vib.* **1995**, *187*, 825–839. [[CrossRef](#)]
28. Fröhling, R. Deterioration of Railway Track Due to Dynamic Vehicle Loading and Spatially Varying Track Stiffness. Ph.D. Thesis, University of Pretoria, Pretoria, South Africa, 1997.
29. Oscarsson, J. Dynamic train-track interaction: Variability attributable to scatter in the track properties. *Veh. Syst. Dyn.* **2002**, *37*, 59–79. [[CrossRef](#)]
30. Berggren, E. Railway Track Stiffness—Dynamic Measurements and Evaluation for Efficient Maintenance. Ph.D. Thesis, KTH Stockholm, Stockholm, Sweden, 2009.
31. Auersch, L. The role of vehicle dynamics in train-induced ground vibrations and the detection of irregular axle-pulse responses due to a varying track stiffness. *Rail Rapid Transit* **2022**, *236*. *accepted for publication*.
32. Auersch, L. Dynamics of the railway track and the underlying soil: The boundary-element solution, theoretical results and their experimental verification. *Veh. Syst. Dyn.* **2005**, *43*, 671–695. [[CrossRef](#)]
33. Auersch, L. Static and dynamic behaviours of isolated and un-isolated ballast tracks using a fast wavenumber domain method. *Arch. Appl. Mech.* **2017**, *87*, 555–574. [[CrossRef](#)]
34. Auersch, L. The excitation of ground vibration by rail traffic: Theory of vehicle–track–soil interaction and measurements on high-speed lines. *J. Sound Vib.* **2005**, *284*, 103–132. [[CrossRef](#)]
35. Auersch, L. Wave propagation in layered soil: Theoretical solution in wavenumber domain and experimental results of hammer and railway traffic excitation. *J. Sound Vib.* **1994**, *173*, 233–264. [[CrossRef](#)]
36. Sheng, X.; Jones, C.; Thompson, D. A comparison of a theoretical model for quasi-statically and dynamically induced environmental vibration from trains with measurements. *J. Sound Vib.* **2003**, *267*, 621–635. [[CrossRef](#)]
37. Auersch, L. Ground vibration due to railway traffic—The calculation of the effects of moving static loads and their experimental verification. *J. Sound Vib.* **2006**, *293*, 599–610. [[CrossRef](#)]
38. Lombaert, G.; Degrande, G. Ground-borne vibration due to static and dynamic axle loads of InterCity and high-speed trains. *J. Sound Vib.* **2009**, *319*, 1036–1066. [[CrossRef](#)]
39. Auersch, L. Train induced ground vibrations: Different amplitude-speed relations for two layered soils. *J. Rail Rapid Transit* **2012**, *226*, 469–488. [[CrossRef](#)]
40. Auersch, L. Fast trains and isolating tracks on inhomogeneous soils. In *Ground Vibrations from High-Speed Railways: Prediction and Mitigation*; Krylov, V., Ed.; ICE Publishing: London, UK, 2019; pp. 27–76.
41. Degrande, G.; Schillemanns, L. Free field vibrations during the passage of a Thalys high-speed train at variable speed. *J. Sound Vib.* **2001**, *247*, 131–144. [[CrossRef](#)]
42. Zhai, W.; Wei, K.; Song, X.; Shao, M. Experimental investigation into ground vibrations induced by very high speed trains on a non-ballasted track. *Soil Dyn. Earthq. Eng.* **2015**, *72*, 24–36. [[CrossRef](#)]